NBS-SNI, an extension of the Network-based statistic: Investigating differences in functional connections between important structural actors in case-control studies

Francis Normand[1,3], **Daniel C. Côté** [1,2], **Antoine Allard**[2,3]

[1]Centre de recherche CERVO, Québec (Québec), Canada G1J 2G3

[2]Département de physique, de génie physique et d'optique, Université Laval, Québec (Québec), Canada G1V 0A6

[3]Centre interdisciplinaire en modélisation mathématique, Université Laval, Québec (Québec), Canada G1V 0A6

Keywords: Brain disorders, Structural Connectivity, Functional Connectivity, Centrality measures

ABSTRACT

Elucidating the coupling between the structure and the function of the brain and its development across maturation has attracted a lot of interest in the field of network neuroscience in the last fifteen years. Mounting evidence support the hypothesis that the interplay between the structural architecture and the functional processes of the brain plays an important role in the onset of certain brain disorders such as schizophrenia and autism. This papers introduces a method called NBS-SNI that integrates both representations into a single framework, and identifies connectivity abnormalities in case-control studies. With this method, significance is given to the properties of the nodes, as well as to the connections between them. This approach builds on the well-established Network-based statistics (NBS) proposed in 2010. We uncover and identify the regimes in which NBS-SNI offers a gain in statistical resolution to identify a contrast of interest using synthetic data. We also apply our method on a real case-control study of individuals diagnosed with autism. Using NBS-SNI and node properties such as the closeness centrality and local information dimension, we found both hypo and hyperconnected subnetworks and show that our method can offer a 9 percentage points gain in prediction power over the standard NBS.

AUTHOR SUMMARY

We propose an extension to the well-known Network-based statistic (NBS) dubbed NBS-SNI. The goal of this approach is to integrate nodal properties such as centrality measures into the statistical network-based framework of NBS to probe for abnormal connectivity between important nodes in case-control studies. We expose the regimes where NBS-SNI offers greater statistical resolution for identifying a contrast of interest using synthetic data and test the approach with a real autism-healthy dataset which contains both the structural (DTI) and functional (fMRI) brain networks of each individual.

1 INTRODUCTION

Shedding light the on the heterogeneous structure-function relationships in the brain has been the aim of many studies over the past ten years (Baum et al., 2017, 2020; Honey,

Thivierge, & Sporns, 2010; Park & Friston, 2013; Pessoa, 2014; Suárez, Markello, Betzel, & Misic, 2020; Witvliet et al., 2021). These endeavors stem from the well established hypothesis in neuroscience that functional activity in the brain should be somehow related to its underlying structural architecture; indeed, the structural connectome is what supports the vast collection of functional patterns available to the human brain (Sporns & Kötter, 2004). Further, another premise in neuroscience is that this cortical plasticity (structural) is mostly apparent in the human brain during youth, which would make it a crucial period for proper cognitive maturation (Baum et al., 2020). These considerations give grounds for investigating the interplay between structure and function in certain brain conditions that onsets during youth or adolescence, such as schizophrenia (Cocchi et al., 2014) and autism (Rudie et al., 2013), through the use of methods such as the one we propose in this paper.

We introduce a procedure called Network-based statistic simultaneous node investigation (NBS-SNI) which incorporates simultaneously two representations of the brain (e.g., structural and functional networks) to identify differences and to perform diagnosis in typical case-control studies. Using synthetic data, we show that incorporating nodal properties extracted from the structural network representations of the brain can enhance the performance at identifying functional abnormalities in case-control studies. More precisely, by considering the principal actors of the structural networks, we show that, in certain regimes, our method can flush out false positives and increase the resolution at which significant edges (true positives) can be identified. As an illustration, using brain networks derived from neuroimaging data of a autism-healthy study (Rudie et al., 2013), where both the structural and functional networks are available ($N = 29$ ASD, $N = 19$ typically developing; TD), we found that NBS-SNI offers an improvement of 9 percentage points in prediction performance (73%) compared to the standard NBS (64%; Zalesky, Fornito, & Bullmore, 2010). NBS-SNI aims to identify differences between two groups (case/control) of brain networks through an examination of abnormal connectivity between the most important actors (nodes) of these networks. It does so by integrating both a structural and a functional network representation of the brain at once, in pursuance of a more comprehensive representation of the brain. Within the proposed NBS-SNI framework, a node property is computed for every node in each network of the healthy and the condition groups, and compared through the lens of statistical testing. Section 2 briefly presents a few nodal properties that will be used within the framework of NBS-SNI. We believe that these properties could capture relevant nodal features related to the notions of efficiency and resilience in brain networks.

2 METHODS

NBS-SNI is an extension to the well established Network-based statistic (NBS; Zalesky et al., 2010), a general framework used to test specific hypotheses in typical case-control studies. In essence, the formulation of NBS-SNI we propose here tries to identify the most important nodes, common to the healthy and condition brain networks, and probes for abnormalities (hyper or hypo) in the interconnection around these influential brain regions. This is different from the standard NBS, which considers the extent to which significant edges (from a t-test perspective) are interconnected to form a component. The notion of component, i.e. retaining only the significant edges that form a connected component, is relaxed with this approach, since an additional restriction comes from the consideration of significant nodes, again by means of a statistical t-test, in addition to significant edges. A node property is computed for every node in the brain networks. The choice of a relevant

node property in the context of brain network analysis is at the liberty of the investigator; a few possibly relevant node measures for network neuroscience are presented in section 2.

It is hypothesized that such a set of edges where stronger connections are observed between *particular* nodes in one group versus the other could be associated with certain symptoms, or network pathologies. Therefore, the choice of an appropriate node measure can be guided by prior knowledge of the specific condition under investigation. The resulting set of connections identified by this approach can then be paired with the framework NBS-predict proposed by Serin, Zalesky, Matory, Walter, and Kruschwitz (2021) to yield a prediction of individuals' classes in case-control studies. In this paper, the relevance (significance) of the subnetworks extracted from real data are assessed by the prediction performances that they yielded on individual brain networks through the use of NBS-predict framework (as opposed to significance being assessed by permutation testing, as it was originally done in Zalesky et al. 2010).

This approach allows the analysis of both structural and functional representations of individual brain networks at once, under a single framework. Owing to the statistical framework of the method, which compares individuals across two representations of brain networks, a perfect node correspondence is required across both representations.

Brain network representations

Depending on the imaging modalities employed, the nodes representing the constituents of the brain network representation could be individual neurons (micro-scale), groups of neurons (meso-scale) or brain regions (large-scale). The interactions (or associations) between the nodes are represented by the edges of the network, and their nature depends on the imaging technique employed. A brain network of n nodes is represented by a $n \times n$ connectivity (or adjacency) matrix, where the entries represent the pairwise associations between every possible pair of nodes.

The real brain networks investigated in this work originate from both fMRI (functional) and DTI (structural) recordings (large-scale) for every individual; micro/meso-scale brain networks will not be discussed here. Interactions measured by DTI structural imaging are bidirectional (undirected) edges whose weight corresponds to the density of white matter fibers connecting two brain regions. Interactions measured by functional imaging are also weighted and bidirectional, but their weight represents a measure of temporal correlation between the recorded dynamic activities between each pairs of parcellated brain regions.

Node properties

NBS-SNI requires the use of a node property, which should be chosen to capture relevant node features related to efficient communication, resilience, clustering, or to the symptoms associated with the specific condition under investigation. Some of these node properties could be the degree, or the betweenness/closeness centrality, as they are well suited for large-scale brain networks dataset, in which the correspondence between the parcellated brain regions (the nodes) is reliable and the volume of each parcellated region does not vary much across individuals (Simpson, Lyday, Hayasaka, Marsh, & Laurienti, 2013). The chosen node property is computed for every node in each network of the healthy and the condition groups, and then compared through the lens of statistical testing. Before getting into the details of these statistical tests, we briefly describe the node properties used here, and explain their relation to the notions of efficiency and resilience in brain networks.

Closeness centrality

The closeness centrality $C_C(v)$ of a node v quantifies how *close* it is, on average, to all the other nodes in the network. It is defined as the inverse of the average shortest path length ℓ_v (Newman, 2018)

$$C_C(v) = \frac{1}{\ell_v} = \frac{n-1}{\sum_u d(u,v)}, \tag{1}$$

where $d(u,v)$ is the shortest distance between u and v. Shortest distance here can be measured in terms of the smallest number of edges crossed to go from node u to node v, or in terms of the minimal "weight" accumulated while getting from nodes u to node v.

The interpretation of closeness centrality is usually one of access of efficiency or independence from potential control by intermediaries (Brandes, Borgatti, & Freeman, 2016). From this interpretation, a node (brain region) of high closeness centrality would be less vulnerable to potential failures of other brain regions to which it is connected; thereby easing efficient rerouting of information along different pathways. In the context of case-control studies of brain networks, this interpretation of the closeness centrality makes it an interesting property to identify important nodes or identify between-group abnormalities. Closeness centrality will be used for both synthetic (see section 3) and real data (see section 4).

We also consider another measure called the current flow closeness centrality (sometimes called information centrality; Stephenson & Zelen, 1989). Contrary to the closeness, this node property does not make the assumption that communication happens solely along shortest paths (geodesics). Instead, information centrality uses all paths, and assigns them a weight based on the information they contain, therefore potentially capturing more subtle effects caused by non-geodesic paths in complex systems. This distinction with the closeness centrality makes it an interesting nodal property to investigate with NBS-SNI's framework. The reader is referred to Stephenson and Zelen (1989) for detailed calculations of this measure. This measure will be used in section4.

Local Information Dimension

The last node property that will be investigated with NBS-SNI in section 4 with real data is called the local information dimension (LID)(Wen & Deng, 2020), a property derived from the local dimension (LD) Silva and da F. Costa (2013). For brain networks, a local definition of dimensionality allows one to quantify the local resilience of the network. The logic behind this statement is that objects of higher dimensionality might be less susceptible to being compromised by a random attack, since higher dimensionality often entails more redundant pathways, i.e., alternative information transmission pathways.

With the LID, the number of nodes within a certain distance l of a central node v are considered using Shannon entropy. The size l represents the number of links starting from the central node v to the boundaries of the box. The LID D_{I_v} is defined as

$$D_{I_v} = -\frac{d}{d\ln l} I_v(l) = -\frac{d}{d\ln l}\frac{n_v(l)}{n}\ln\left(\frac{n_v(l)}{n}\right), \tag{2}$$

where $I_v(l) = \frac{n_v(l)}{n}\ln\left(\frac{n_v(l)}{n}\right)$ is the information contained in the box of size l whose central node is v, $n_v(l)$ is the number of nodes in a box of size l whose central node is v, while n is

the total number of nodes in the network. With this measure, a larger value indicate a more "influential" node.

The LID D_{I_v} of a node v is obtained from the slope fitting of $I_v(l)$ versus $\ln l$. In contrast to the LD, the size of the box l with LID varies from one to half of the maximum shortest distance from the central node v. This reduces the computational complexity and focuses on the *quasilocal* organization around the central node v. The LID was chosen over the LD as a node property to investigate in this paper owing to its reduced computational complexity, its greater effectiveness and reasonability at identifying influencers in complex networks (Wen & Deng, 2020). Additionally, we found that using the LID as a node property resulted in more accurate predictions than the (more global) local dimension (LD) (Silva & da F. Costa, 2013).

To generalize the LID for weighted networks, a straightforward strategy would be to discretize the l space into an arbitrary number of steps, starting from the minimum weighted shortest distance to half the maximum weighted shortest distance from the central node. This strategy was employed when using this node property in section 4.

NBS-SNI

As formulated in this paper, the method is designed to identify the most important nodes (brain regions) common to both the condition and the control group in the structural representation, and probe for hyperconnected (or hypoconnected) functional connections between these brain regions.

In what follows, both the structural and functional connectivity matrices are available for each individuals in both groups. Moreover, the method assumes that there is a "perfect" correspondence between the nodes across the networks for both representations (*node-aligned networks*).

The method

Let there be N_1 pairs of networks (functional and structural) of n nodes in group 1 (condition) and N_2 pairs of networks of n nodes in group 2 (control). To find significant nodes common to both the condition and control group, a node property is computed for each node from the structural connectivity matrices. This results in a $N_1 \times n$ matrix where each row contains the node measures of all the nodes in a structural network from group 1. The same procedure is done with the other group to obtain a $N_2 \times n$ matrix of node properties (step 1 on Fig. 1). A one-sample t-test is then performed on this property, yielding two vectors of length n containing the t-statistic of each node, one vector for each group (step 2). A threshold t_{node} is then applied to the resulting t-statistics independently in each group to identify significant nodes, and the intersection between the significant nodes of both groups is taken (step 3). This will result in a set of *suprathreshold nodes*, i.e., the important nodes that are common to both groups. These suprathreshold nodes correspond to the most important actors (nodes) of these networks mentioned earlier.

In parallel, a two-sample t-test is also performed on the edge weights of the functional connectivity matrices for a between-group difference (step 4), resulting in a single $n \times n$ matrix that contains the t-statistic of each edge weight as its entries. A threshold is then applied to this matrix (step 5), resulting in a set of suprathreshold edges (step 6).

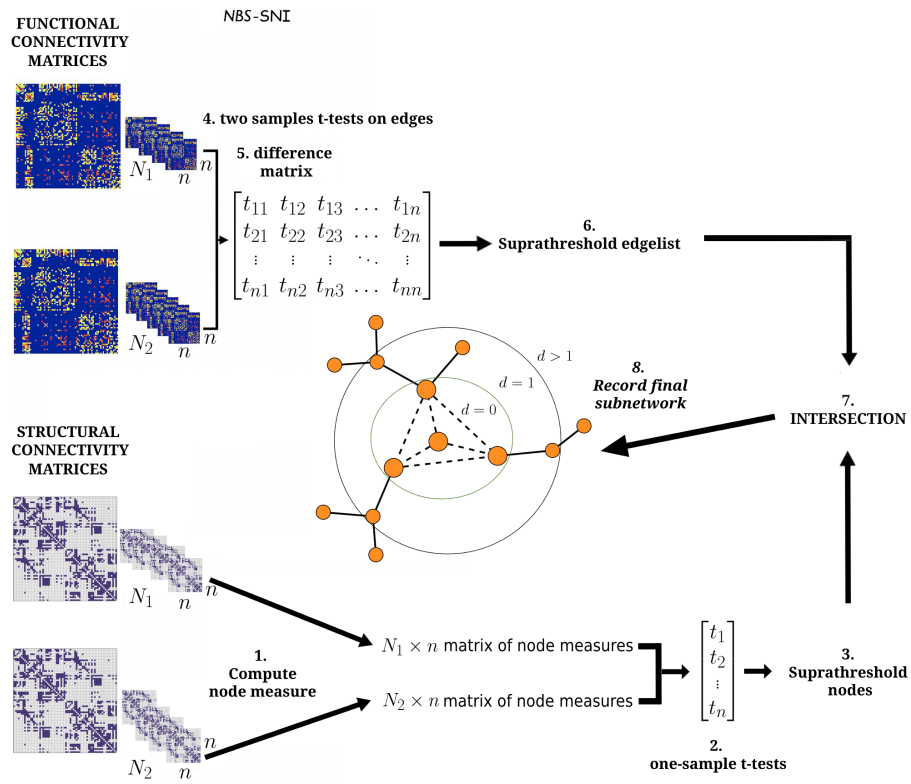

Figure 1. Illustration of NBS-SNI. The inputs are the structural and the functional connectivity matrices, two matrices for each individual in the condition and in the control groups. Statistical tests are performed in parallel on both sets of matrices (structural and functional). On the functional representation, a two-sample t-test is performed on the entries of the connectivity matrices (edge weights) (step **4**), which are then thresholded (step 5), yielding a set of suprathreshold edges (step 6). On the structural representation, a node measure is computed for every node (step **1**), and a one sample t-tests is performed on theses node measures (step **2**) independently for each group. Both sets of nodes' t-scores are then thresholded, and the intersection between the resulting sets is taken (step **3**), thus retaining only the nodes that were statistically significant in both the condition and the control groups. Finally, the intersection ($d = 0$) (or a relaxed intersection ($d \geq 1$)) (step **7**) between the suprathreshold nodes and the suprathreshold edges is taken, and the final set of edges remaining is recorded (step **8**). The three cases considered shown above in the center are $d = 0$, $d = 1$ and $d > 1$, where d is the distance of a node from the central nodes, which are depicted slightly larger.

Finally, the intersection between the resulting suprathreshold nodes and suprathreshold edges is taken (steps 7 and 8). Three cases naturally arise. The most restrictive case consist in retaining only the edges that are shared between the "important" nodes ($d = 0$). Note that for $d = 0$, the subnetwork yielded by NBS-SNI is always a connected component. The second case implies retaining all edges that connect at least one suprathreshold node ($d = 1$). The third case retains edges that connect nodes that are at most at a distance $d > 1$ from the suprathreshold nodes. Note that this third case requires computing shortest distances from the central nodes, which increases the computational complexity of the method.

Hereinafter, we chose to perform the statistical test on the edge weights of the functional connectivity matrices, while the statistical test on the node properties takes place on the

structural connectivity matrices, but swapping these choices could be valid as well. Also, note that an alternative formulation where the investigator first probes for abnormalities in the nodes from the structural representation could also be valid, as opposed to finding nodes considered important for both the condition and control groups.

In our simulations presented in section 3, NBS and NBS-SNI are sometimes compared against the false discovery rate (FDR), i.e. the expected ratio of false positives among all the positives, which serves as a link-based controlling procedure. With FDR, every edge's t-score is treated independently, as opposed to NBS or NBS-SNI, which do not yield a collection of individual significant edges, but rather a connected component that they form.

Classification

We adapted the framework NBS-predict (Serin et al., 2021) to investigate the impact information about nodes taken into account by NBS-SNI has on the accuracy of a classification task. In this context, individual brain networks (functional connectivity matrices) are classified (diagnosed) into either the control or the condition group. The edge weights of the subnetworks extracted by the method are the features which are fed to various machine learning (ML) algorithms (the features associated to the edges that were not selected are set to 0). A K-fold cross validation procedure is repeated r times (see figure 2). Finally, the method outputs an average prediction accuracy for the brain networks and a weighted adjacency matrix, in which the weights of the edges represent their individual prediction accuracy across folds. Figure 2 illustrates the workflow of the classification procedure NBS-predict.

To visualize the contribution of each edge to the overall prediction performance, the selected edges in the extracted subnetworks across folds are constantly updated and assigned a weight (encoded in a single weighted adjacency matrix), which corresponds to the prediction performance at that specific fold (here again, edges that are not selected are assigned a weight of 0). In the end, all the weights are averaged and rescaled so that the maximum prediction weight is 1. One may then visualize the selected edges across folds that contributed the most to the prediction (i.e., the largest weights denote the edges that had a greater prediction accuracy and that were selected the most across folds).

The classification ML algorithms employed in this work are Ridge Classifier, Random Forest Classifier, Decision Tree, Support Vector Machine (SVM) and Logistic Regression, all implemented from the scikit-learn (Pedregosa et al., 2011) Python package.

3 CONTRAST IDENTIFICATION: NBS-SNI VS. NBS USING SYNTHETIC DATA

To compare the statistical resolution of NBS-SNI with NBS to identify a contrast, synthetic data was created for both structural and functional connectivity brain networks in a typical case-control study setup. As mentioned previously, we expect NBS-SNI to draw its strength from considering both representations simultaneously, when an interplay of contrasts exists across the two representations.

Synthetic data model

Generative model for the structural networks

Our approach to generate synthetic structural networks is inspired by Akarca, Vértes, Bullmore, and Astle (2021); Betzel et al. (2016) and goes as follows. Edges are added one at a

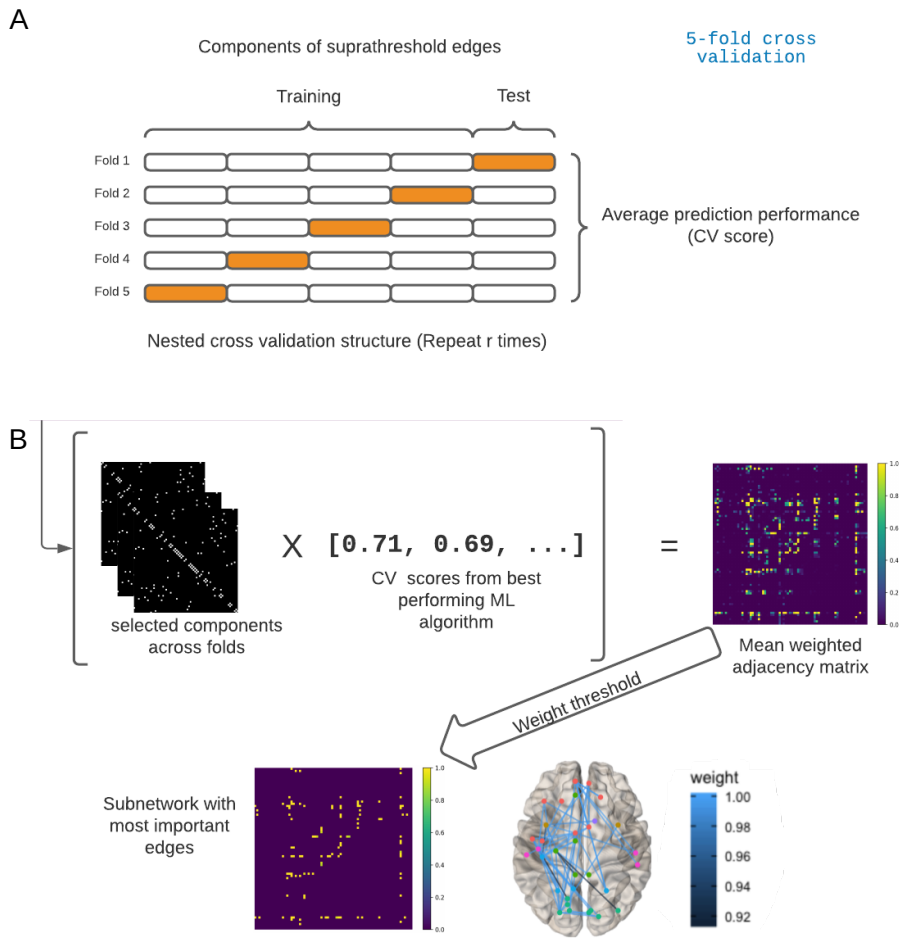

Figure 2. Illustration of the process employed for the classification task. A. Nested cross-validation structure (K = 5 folds in this example) employed to yield out-of-sample predictions. A nested cross validation is one that is repeated r times. This is done to take into account possible variations in the prediction performances in the test subsets. B. The framework of NBS-predict (Serin et al., 2021). The subnetworks binary adjacency matrices obtained across folds are multiplied with their associated prediction performance. This procedure outputs a weighted adjacency matrix, which holds the relative importance of each edge in making predictions across the nested cross-validation process. It is then possible to apply a threshold to the resulting weighted adjacency matrix to retain and visualize only the edges that contributed the most to the predictions. This illustration is inspired by Fig 1 from Serin et al. (2021).

time probabilistically until the desired number of edges has been added. The probability of forming an edge between node u and node v is given by

$$P^{\text{structural}}(u,v) = E(u,v) \times K(u,v), \tag{3}$$

where $E(u,v)$ represents the probability of connection between brain regions u and v, depending on the Euclidean distance d_{uv} separating them. The second term $K(u,v)$ assigns a greater probability of connection on the preselected set of nodes, n_c, defined as the contrasting nodes, or alternatively adds noise to the connection probability between the other nodes. These rules for $K(u,v)$ are expressed as

$$K(u,v) = \begin{cases} K_{n_c}(u,v) \sim \mathcal{N}(\mu_{n_c}, \sigma_{n_c}) & \text{if either } u \text{ or } v \text{ belongs to } n_c \\ \delta_{\text{noise}} \sim \mathcal{N}(0, \sigma_{n_c}) & \text{otherwise.} \end{cases} \tag{4}$$

By increasing the connection probability between u and v if either belongs to n_c, the last term in Eq. 3 effectively increases the closeness centrality of the nodes in n_c compared to the other nodes. In accordance with the formulation of NBS-SNI we propose in this paper, both groups of synthetic brain networks (condition and control) were induced the same high centrality nodes, i.e., the high centrality nodes in n_c were common to both groups of networks. The nodes in n_c serve as the important actors previously mentioned. Note that all connections are bidirectional, i.e., when a connection is added from node u to node v, the same connection is also added from node v to u. Note also, that an edge can only be added once, therefore the probabilities are adjusted accordingly during the generative process.

To obtain the parameters associated with $E(u,v)$, we plotted the probability of connection P_{uv} between node u and v for the real structural network dataset of 264 brain regions (UCLA Autism; Rudie et al., 2013) as a function of the distance separating them d_{uv}, considering both groups (ASD and control networks) altogether. We found that this relationship could be closely approximated by three different functions according to the range of distances. For distances ranging from $d_{uv} = 0$ up to $d_{uv} = 18$mm, a function a of the form $P_{uv} \propto A_1 \frac{\log d_{uv} - b}{d_{uv} - b}$ was fitted. The second part was approximated using a function of the form $P_{uv} \propto A_2 e^{-\ell d_{uv}} (d_{uv})^{-\eta_2}$ for distances ranging from $18 \leq d_{uv} < 39$mm. For the last part ($d_{uv} \geq 39$), a power law of the form $P_{uv} \propto A_3 (d_{uv})^{\eta_3}$ was fitted.

Since structural brain networks are generally represented as weighted networks, the distribution of weights from the real autism structural dataset was also extracted. We found that a function of the form $p_w \approx \alpha_w \cdot e^{(kw)}/w + C_w$, where p_w is the probability of finding a connection with weight w between two brain regions was a good approximation of the first half of this relationship. The second half (the right tail) of this relationship was approximated by a power law distribution $\propto A_w \cdot w^{-\eta_w}$, which allows for a few larger connection weights that cannot be accounted for by the first function ($A_w \cdot e^{(kw)}/w$).

For $E(u,v)$, the parameters we found empirically are: (first part;$A_1 = 133.49$ and $b = -899.3$), (second part; $A_2 = 0.000943$, $\ell = 0.2277$ and $\eta_2 = -3.83$) and (third part; $A_3 = 275.178$ and $\eta_3 = 2.031$). For the weights, we found $\alpha_w = 0.194$, $k = 1.038 \times 10^{-6}$ and $C_w = -0.0007$ for the first part, and $A_w = 627.78$ and $\eta_w = 2.99$ for the second part. Moreover standard deviation $\sigma_{n_c} = 2$ was kept constant for all our experiments.

Functional network generative model

The synthetic functional brain networks are fully connected undirected weighted networks, i.e., a bidirectional weighted connection exists between every pair of nodes (u, v).

In one group (noise+contrast(s) group), the entries of the adjacency matrices can comprise different contrasts of connections on different sets of edges $n_e^{(i)}$ sampled from $\mathcal{N}(\mu_e^{(i)}, \sigma)$, while the other connection weights (noise) are sampled from $\mathcal{N}(0, \sigma)$. The probability density function for the weights thus is

$$w^{\text{functional}}(u, v) = \begin{cases} w \sim \mathcal{N}(\mu_e^{(i)}, \sigma) & \text{if the edge } (u, v) \text{ belongs to } n_e^{(i)} \\ w \sim \mathcal{N}(0, \sigma) & \text{otherwise.} \end{cases} \tag{5}$$

In the other group (noise only group) all the entries in the adjacency matrices are sampled from $\mathcal{N}(0, \sigma)$. For $\sigma = 1$ (the value employed for all the functional contrasts in our simulations), this procedure has the effect of creating a contrast-to-noise ratio CNR $= \mu_e^{(i)}$ on the edges in $\mu_e^{(i)}$ in one group, while the other group consists of adjacency matrices with all their entries sampled from Gaussian noise of zero mean and variance σ^2.

Numerical experiments

Identification of an embedded contrast

The synthetic networks for this experiment were built using the same nodes ($n = 264$; including their positions) as in the UCLA Autism dataset (Rudie et al., 2013), of which $|n_c| = 5$ were chosen as being more central (see Fig. 3A). The same number of weighted edges, 3188, were randomly added using Eq. (3), with parameters $\mu_{n_c} = 1.5$ and $\sigma_{n_c} = 2$. We generated 60 synthetic structural networks equally divided into the condition and the control groups, each network consisting in a single connected component.

To build the functional networks from the condition group, a first set of 8 edges connected to at least one node in n_c were given a weight using Eq. (5) with $\mu_e^{(1)} = 0.6$ and $\sigma = 1$ (subcontrast edges; dashed lines in Fig. 3B). A second set of 11 edges located in the periphery of the 5 nodes in n_c were given a weight using Eq. (5) with $\mu_e^{(2)} = 0.8$ and $\sigma = 1$ (contrast edges; solid lines in Fig. 3B). All other edges, as well as all edges in the functional networks belonging to the control group, were given a weight according to Eq. (5) (sampled from $\mathcal{N}(0, 1)$).

Our objective here is to illustrate how taking into account information about the nodes (here present in the structural networks) can allow the identification of edges that do not necessarily have the largest contrast-to-noise ratio (these subcontrast edges are shown in Figs. 3C and 4A). Figure 4 shows a comparison of the performances between NBS and NBS-SNI with $d = 1$.

Blue edges correspond to connections identified by either method that did not belong to the subcontrast (false positives), while red edges correspond to connections that were missed (false negatives) Figure 4B shows the results for two sets of parameter thresholds t_{edge} obtained with NBS-SNI, which perfectly recovers the subcontrast edges. Figure 4C shows that t_{edge} could not be tuned for NBS to perfectly recover the subcontrast edges.

Figure 4 illustrates what was already expected owing to the design of NBS-SNI, i.e., it can recover a subcontrast that is embedded inside another contrast of greater CNR, a task NBS is not suited for. Evidently, this conclusion is only valid if the nodes in the subcontrast share

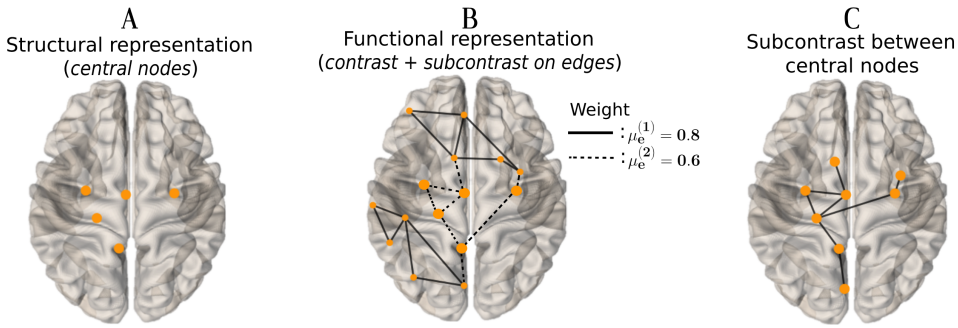

Figure 3. This synthetic data consists of network models of 264 nodes with 30 networks in each group. **A** Illustration of the 5 nodes in n_c on which a greater closeness centrality score was induced in the structural network models with $K_{n_c}(u,v) \sim \mathcal{N}(1.5, 2)$. **B** Illustration of the functional connected component created around the 5 central nodes. Edges with a lower CNR sampled from $\mathcal{N}(0.6, 1)$ are depicted as dashed lines, while edges belonging to the contrast of greater CNR sampled from $\mathcal{N}(0.8, 1)$ are represented by solid lines. The five central nodes in n_c are depicted bigger. **C** The subcontrast, i.e., the connections of lower CNR interconnecting the 5 central nodes and reaching three other nodes placed at a maximum distance $d = 1$ from the central ones (now represented as solid lines).

some common property (e.g., the closeness centrality in this example), which distinguishes them from the other nodes. In our example, this shared property between the nodes in the subcontrast was induced in the structural network models, but a nodal property could also be computed from the functional network representations. We chose this formulation since nodal properties based on shortest distances seem most suited for structural networks than for functional ones.

Systematic comparison

The next experiment aims at getting a better grasp of the cases when NBS-SNI offers a gain over NBS (and when it does not). Alongside the specificity and sensitivity of both NBS-SNI and NBS, we also consider the false discovery rate (FDR) to compare the two methods with a link-based controlling procedure.

Indeed, FDR treats every edge independently, as opposed to NBS and NBS-SNI, which cannot declare individual edges to be significant, but rather the component that they form. We evaluated the specificity and sensitivity of both NBS-SNI and NBS, along with the false discovery rate (FDR).

The experiment goes as follows. This procedure is to be repeated 1000 times for each set of parameters and thresholds (see Fig. 5 for details). Again, synthetic networks were built using the 264 nodes and their pair of distances from the UCLA Autism dataset (Rudie et al., 2013). Among these nodes, $|n_c| = 5$ are randomly selected to be the central nodes in the structural network. Among the $\binom{|n_c|}{2}$ edges between these nodes and two other nodes (not present in n_c) in the functional networks, a component of 20 edges consisting of a single contrast with mean CNR $\mu_e^{(1)}$ and variance $\sigma = 1$ is selected as the set $n_e^{(1)}$. The component of functional edges therefore encompasses the five central nodes, plus two other nodes which do not possess higher induced centrality. Using Eqs. (3) and (5), 60 synthetic

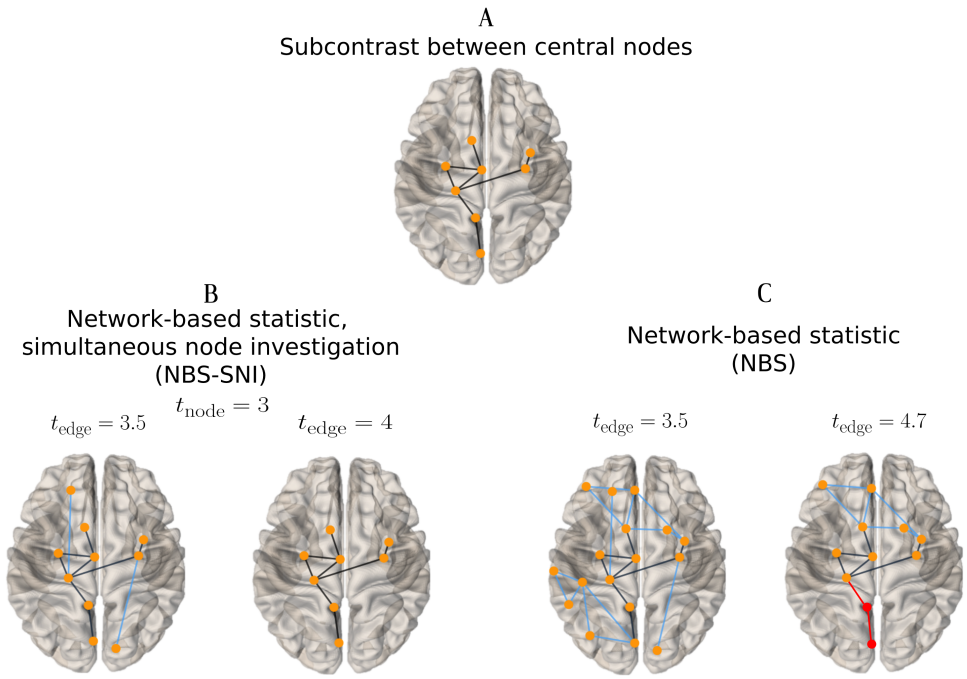

Figure 4. NBS-SNI and NBS performances at identifying a subcontrast were compared on the simulated data shown in figure 3, for two sets of parameter thresholds. **A** The target subcontrast to be identified (a reproduction of figure 3C. **B** The subnetworks extracted with NBS-SNI across two different thresholds t_{edge}. NBS-SNI perfectly recovers the simulated subcontrast. **C** The subnetwork extracted by NBS, which fails to perfectly capture the subcontrast, with 5 false positive and 2 false negative connections.

networks equally divided into the condition and the control groups are generated. (Recall that edges in the set $n_e^{(1)}$ in the functional networks associated with the control group are no different than the other edges.) The most significant edges are then identified using the three methods (using $d = 1$ for NBS-SNI) and the true positive (TPR) and false positive rates (FPR) are computed. For NBS-SNI, $d = 1$ was used since some of the 20 connections in the contrast reach two nodes that do not belong to n_c.

The results are summarized by means of the receiver operating characteristic (ROC) curves shown in Fig. 5. In all cases, the value of the parameter thresholds ranged from $t_{\text{edge}} = 0.5$ to $t_{\text{edge}} = 6$ (for NBS-SNI and NBS) and $q = 0.001$ to $q = 0.99$ (for FDR; q-values represent the expected false discovery rate), with 100 equally spaced values in-between. For NBS-SNI, the parameter threshold for the nodes was kept constant at $t_{\text{node}} = 0.5$ for all realizations. For the synthetic functional networks, all the edge weights were sampled from a Gaussian distribution with with $\mu = 0$ and $\sigma = 1$.

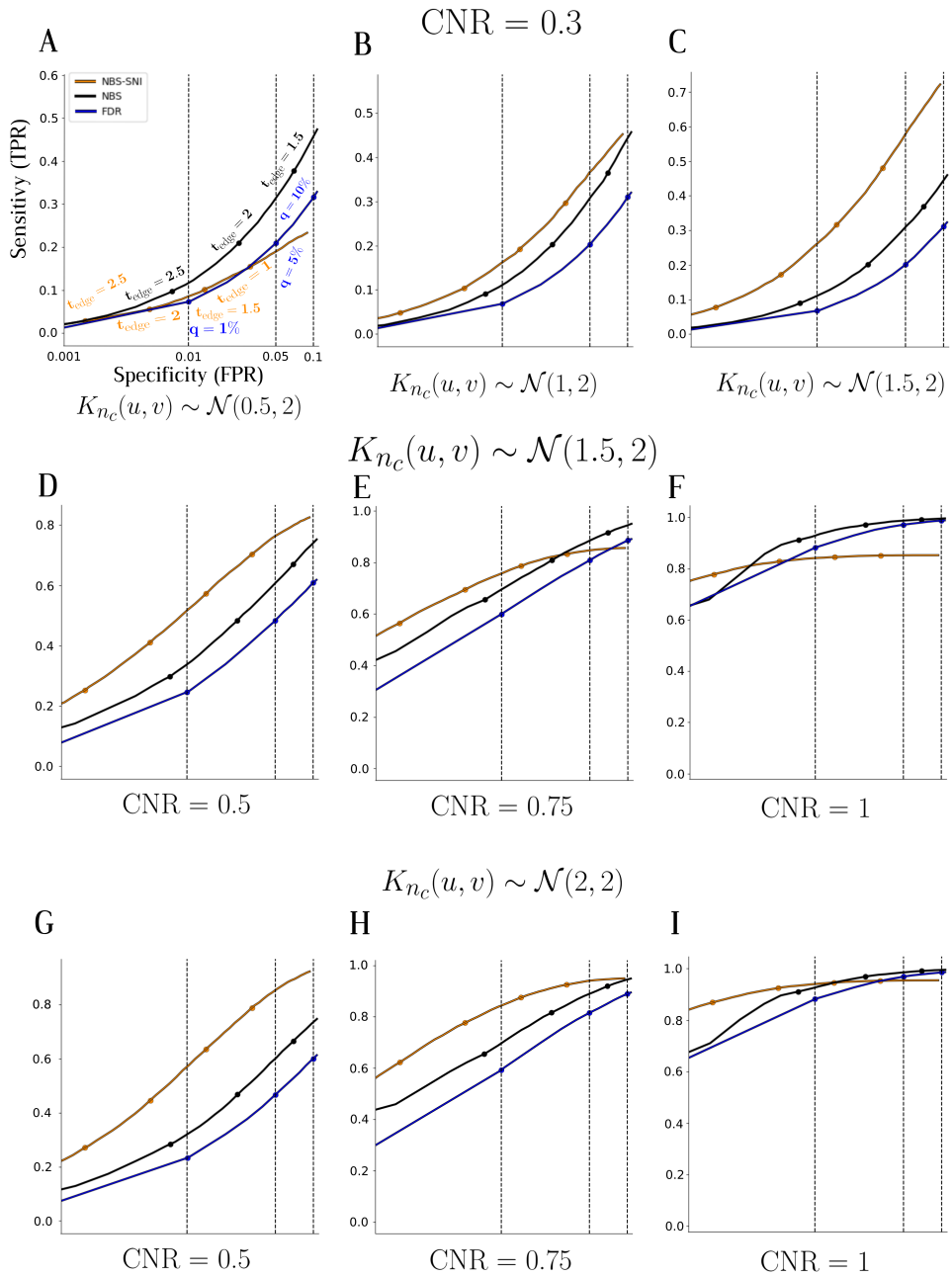

Figure 5. Receiver operating characteristic (ROC) curves were plotted to compare the sensitivity (TPR) and specificity (FPR) of NBS-SNI (orange), NBS (black) and the false discovery rate (FDR) (blue), serving as a link-based controlling procedure, in detecting a simulated contrast on synthetic networks. Each point on a ROC curve for NBS-SNI and NBS (orange and black curves, respectively) represents the average of the TPR and FPR calculated from the 1000 realizations, at a specific parameter threshold t_{edge}, some of which are indicated on the curves. For the FDR curves (in blue), each point represents a different q-value threshold, with a few indicated as a percentage. **A** ROC curves with the parameters $w \sim \mathcal{N}(\mu_e^{(1)} = 0.3, \sigma = 1)$ in the functional network models and $K_{n_c} \sim \mathcal{N}(\mu_{n_c} = 0.5, \sigma_{n_c} = 2)$ in the structural network models. **B** ($\mu_e^{(1)} = 0.3$; $\sigma = 1$) and ($\mu_{n_c} = 1$; $\sigma_{n_c} = 2$). **C** ($\mu_e^{(1)} = 0.3$; $\sigma = 1$) and ($\mu_{n_c} = 1.5$; $\mu_{n_c} = 2$). **D** ($\mu_{n_c} = 1.5$; $\mu_{n_c} = 2$) and ($\mu_e^{(1)} = 0.5$; $\sigma = 1$) **E** ($\mu_{n_c} = 1.5$; $\mu_{n_c} = 2$) and ($\mu_e^{(1)} = 0.75$; $\sigma = 1$). **F** ($\mu_{n_c} = 1.5$; $\mu_{n_c} = 2$) and ($\mu_e^{(1)} = 1$; $\sigma = 1$). **G** ($\mu_{n_c} = 2$; $\mu_{n_c} = 2$) and ($\mu_e^{(1)} = 0.5$; $\sigma = 1$). **H** ($\mu_{n_c} = 2$; $\mu_{n_c} = 2$) and ($\mu_e^{(1)} = 0.75$; $\sigma = 1$). **I** ($\mu_{n_c} = 2$; $\mu_{n_c} = 2$) and ($\mu_e^{(1)} = 1$; $\sigma = 1$).

In figure 5A-C, the parameter μ_{n_c} in $K_{n_c}(u,v) \sim \mathcal{N}(\mu_{n_c}, \sigma_{n_c} = 2)$ was varied in the structural network models for a given CNR = 0.3 ($\mu_e^{(1)} = 0.3$; $\sigma = 1$) between the two groups in the functional network models. Since only the properties of the structural models are altered, NBS and FDR's performances remain the same across figures 5A-B-C. It is only the performance of NBS-SNI that improves, i.e. the curves' ascension is steeper, as the parameter μ_{n_c} in the structural model is increased.

Figure 5D-F shows the ROC curves for three different CNRs in the functional network models, for a constant parameter $\mu_{n_c} = 1.5$ in the structural network models. The gain in statistical resolution offered by NBS-SNI compared to the others becomes less significant as the CNR is increased.

In figure 5G-I, the CNR was again varied, but for a constant structural model parameter increased to $\mu_{n_c} = 2$. On the right, figure 5F with CNR = 1, all three methods offer similar performances after FPR = 0.01, thereby showing the gain in statistical resolution of NBS-SNI and NBS over FDR to be most effective at lower contrast-to-noise ratios (Zalesky et al., 2010).

The following takeaway points from figure 5 pertain only to cases where the contrast forms a component and interconnects nodes that share a common property of interest (for e.g., high centrality nodes): (1) as the CNR (μ_c) gets smaller, the better is the statistical resolution offered by NBS-SNI compared to NBS and FDR. (2) The more pronounced is the node property of interest (parameter μ_{n_c}) in the structural data, the greater is the statistical resolution offered by NBS-SNI. (3) As the CNR is increased and μ_{n_c} remains constant, the standard NBS and FDR will at some point offer a better resolution than NBS-SNI.

In sum, NBS-SNI offers a tighter control of the family-wise error rate than the other two methods in certain regimes by considering the nodes themselves, as opposed to considering only the edges. By giving importance to the nodes, the investigator can lower the parameter threshold t_{edge} to find significant abnormal connections of lower CNR. Conversely, the investigator could keep the same parameter threshold t_{edge} with NBS-SNI, thereby eliminating potential false positives that would result using NBS with the same value of t_{edge}. This choice would depend on the desirable trade-off between finding true positives and eliminating false ones.

The results presented in the ROC curves of figure 5 offer a somewhat narrow view of the discriminating performances of the different methods, owing to the specific parameters employed in each simulation. A more comprehensive interpretation of these results is given in figure 6, where the relative performances of NBS-SNI and NBS are shown when varying the number of samples and the overlap coefficient (OVL) between the Gaussian noise $\mathcal{N}(0,1)$ and the contrast $\mathcal{N}(\mu_e^{(1)}, 1)$ (the standard deviation was again kept constant at $\sigma = 1$ for all realizations). The OVL measures the similarity between two distributions via the overlapping area of their distribution functions. As for the ROC curves in figure 5, N ($N_1 = N_2$) networks were generated in each group, with a contrast of only 10 functional edges. To accelerate the computations, synthetic networks were built using the first $n = 100$ nodes in the UCLA Autism dataset (Rudie et al., 2013), which covers only and most of the posterior cortex. Among these nodes, $|n_c| = 7$ are randomly selected to be the central nodes in the structural network.

To ensure a fair comparison of the true positive rate yielded by NBS-SNI and NBS, we controlled for the number of significant edges yielded by both methods. Their perfor-

mances were compared based on subnetworks containing exactly 50 edges. To enforce this, the 200 (300) most significant t-scores with NBS (NBS-SNI) were retained and the largest connected component identified. For NBS, the top 50 most significant t-scores within the remaining connected component were retained. The same was done with NBS-SNI after taking the relaxed intersection ($d = 1$) with the central nodes ($t_{\text{node}} = 0.5$).

The orange circles represent a pair of parameters (number of samples, OVL) for which NBS-SNI offered a better performance ($\text{TPR}_{\text{SNI}} > \text{TPR}_{\text{NBS}}$), where their sizes and colors reflect the relative gain in statistical resolution compared to NBS. The relative importance (in both color and size) of each point is calculated as $\text{TPR}_{\text{SNI}} - \text{TPR}_{\text{NBS}}$. For visualization purposes, a colormap was not used for NBS, i.e. when $\text{TPR}_{\text{NBS}} > \text{TPR}_{\text{SNI}}$ (black triangles); only the size of the triangles reflects the relative gain in statistical resolution offered by NBS over NBS-SNI.

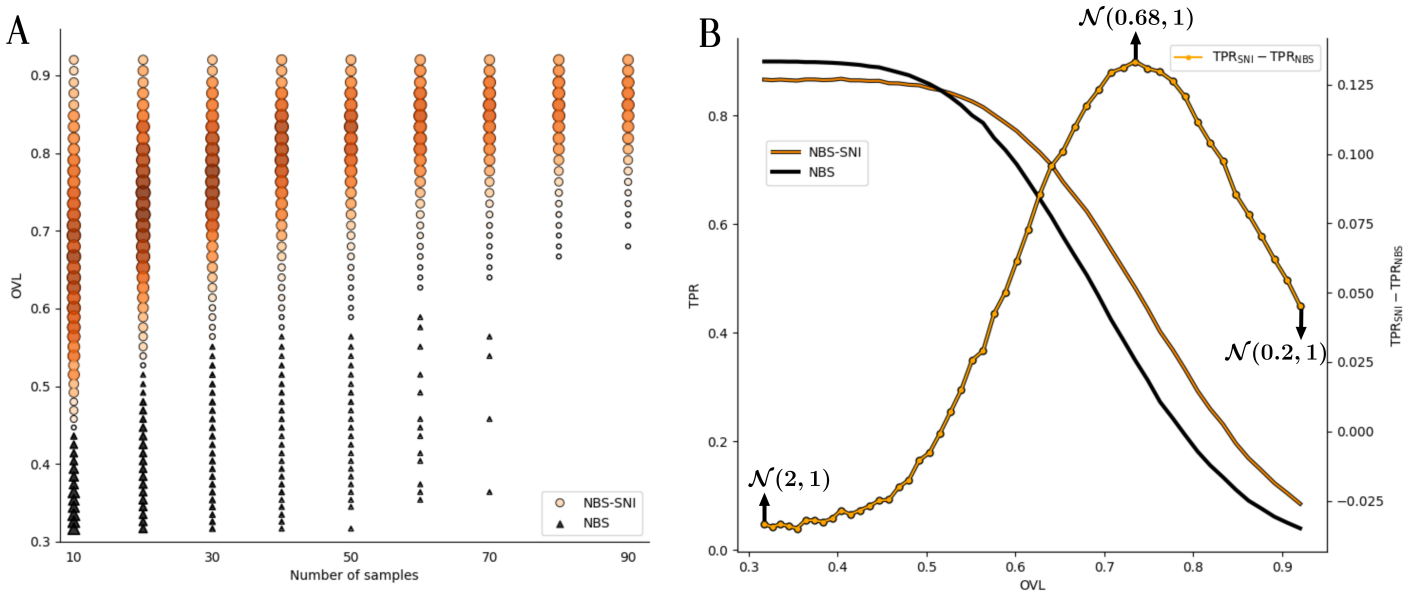

Figure 6. **A** Relative performance of NBS-SNI versus NBS at identifying a contrast of 10 edges in networks of 100 nodes as a function of the overlap coefficient (OVL) and the number of synthetic network samples generated in each group. Orange circles represent a set of parameters where NBS-SNI offered a greater true positive rate (TPR) than NBS, while black triangles show the cases where NBS yielded a greater TPR than NBS-SNI. For NBS-SNI, the size and color intensity of the points represents the relative gain in statistical resolution over NBS, calculated as $\text{TPR}_{\text{SNI}} - \text{TPR}_{\text{NBS}}$. A color map was not used for the cases where $\text{TPR}_{\text{NBS}} - \text{TPR}_{\text{SNI}}$ for a clearer visualization; only the size of the black triangles reflects the gain in resolution. **B** TPR as a function of the overlap coefficient (OVL) for 20 samples, along with the curve showing the difference between the two performances, calculated as $\text{TPR}_{\text{SNI}} - \text{TPR}_{\text{NBS}}$. The orange (NBS-SNI) and black (NBS) curves correspond to the second column from the left in A.

The results from figures 5 and 6 indicate that NBS-SNI can improve the statistical resolution in certain regimes by considering two representations simultaneously. More precisely, we expect NBS-SNI to outperform NBS at identifying a contrast of *relatively* small contrast-to-noise ratio (CNR) in the functional network representations, where the nodes

comprised in this contrast manifest themselves as high centrality nodes in the structural network representations of both groups. The intuition for proposing this kind of synthetic data is that some brain regions (nodes) could manifest as important information carrier (central nodes) in the structural representation of both the condition and the control group, while the arrangement and the strength of the connections emanating from these central nodes may differ in the functional representation. In other words, the synthetic data model employed is such that the identity of some high centrality nodes is common to both groups (condition and control) in the structural networks, but the functional connections between theses nodes may vary across the two groups. By relatively small, we mean that the CNR is smaller than the standard deviation of the modelled Gaussian noise.

Such a configuration may allow us to be less restrictive on the threshold applied to the set of edges in the functional networks. Since NBS-SNI is also concerned with high centrality nodes, which are retained from the statistical test applied to the structural network representations, acknowledging central nodes in our framework might help us throw out some false positive edges that could have been retained from the functional edges' statistical test. We posit that the false positive rate can be lowered in such a case with NBS-SNI, while the true positive rate can be increased as seen in figure 6.

4 BRAIN NETWORK CLASSIFICATION PERFORMANCES OF NBS-SNI VS. NBS USING REAL CASE-CONTROL DATA

In this section, we present the results obtained with NBS-SNI applied to a real case-control study, which consists of individuals diagnosed with the autism spectrum disorder (ASD). The procedure employed to yield predictions is detailed in section 2. All the machine learning algorithms paired with NBS-SNI used to perform predictions are the ones implemented by the Python package scikit-learn (Pedregosa et al., 2011), without any hyper-parameters optimization.

Sample characteristics

This dataset consists of 29 individuals diagnosed with ASD and 19 healthy individuals. Each individual in both groups is represented by a structural connectivity matrix and a functional connectivity matrix (resting-state). Moreover, there exists a node correspondence between all 264 nodes (mapped according to the Power264 brain atlas of Power et al. 2011) across both groups and both representations. The functional network representations are fully connected and weighted networks, where an edge represents the pairwise correlation between two brain regions. These structural networks are sparse weighted and undirected networks, where an edge represents the density of white-mater axonal fiber tracts between two brain regions.

Results and Discussion

We used NBS-SNI with $d = 1$ (i.e., edges at a maximal distance of 1 from the central nodes are retained), paired with the machine learning and cross-validation procedure described earlier to perform classification of brain networks in a case-control setup. Brain networks are classified in either the ASD or control group. The parameters $K = 15$ and $r = 25$ were employed for the repeated k-fold cross-validation.

Closeness centrality

The first node property investigated with NBS-SNI is the closeness centrality C_C (see section 2). The classification results obtained with different machine learning algorithms are presented in Table 1. The best prediction performance was yielded by the Logistic Regression algorithm ($\mu_{\text{performance}} = 0.670 \pm 0.053$) with the hyperconnected subnetwork, i.e., a hyperconnected subnetwork in the autism group of brain networks, containing an average of $k_{\text{hypo}} = 188 \pm 20$ functional connections across folds.

For the hyperconnected case with the Logistic regression algorithm, applying a weight threshold of 1 to the final adjacency matrix containing the average prediction weight of every edges across folds as its entries, 23 hyperconnected edges remained. A hyperconnected component of 11 edges was identified within these 23 edges. The hyperconnected component is depicted in figure 7, alongside the list of its nodes and their associated degree. Interestingly, most of the connections are lateral (across hemispheres), with a larger proportion reaching the right putamen.

Current flow closeness centrality

A variant of the closeness centrality, called the current flow closeness centrality (or sometimes information centrality) was also employed with NBS-SNI. The prediction performances with this node property are presented in table 2. The best performance was yielded by the Ridge classifier algorithm ($\mu_{\text{performance}} = 0.734 \pm 0.039$) using the hypoconnected subnetwork, i.e., a disconnected subnetwork in the autism group of brain networks containing an average of $k_{\text{hyper}} = 227 \pm 26$ functional connections.

Applying a weight threshold of 0.99 to the final prediction adjacency matrix (yielded with the Ridge classifier algorithm) yielded 43 hypoconnected edges. Within these 43 edges, a hypoconnected components of 23 edges was identified, which is shown in figure 8, alongside its nodes and their degree. Most connections seem to converge near the center of the sagittal plane of the brain. Notably is the large number of connections reaching the brain-stem, the right cingulate gyrus posterior division and the right precuneous cortex. Together, these three brain regions account for 46% of all the connections implicated between all 20 brain regions of the hypoconnected component.

Local information dimension (LID)

Finally the local information dimension (see 2) was employed as the node property with NBS-SNI. To employ this node measure with the weighted networks of the structural representations, the sizes of the box l around a node was discretized into 15 equally spaced parts between the minimum distance and half of the maximum weighted distance between two nodes within the network for which the node's LID are being computed. The prediction performances are presented in table 3. The best performance was yielded by Decision tree classifier algorithm ($\mu_{\text{performance}} = 0.704 \pm 0.063$), using the hyperconnected subnetwork, containing on average $k_{\text{hypo}} = 123 \pm 18$ functional connections.

Applying a weight threshold of 0.99 to the final prediction adjacency matrix yielded by the Decision tree classifier algorithm resulted in 17 hyperconnected edges. Within these 17 edges, the hyperconnected component of 10 edges was identified and is depicted in figure 9, alongside the nodes and their degree. The majority of the nodes involved in the hyperconnected subnetwork are localized in the right hemisphere, connecting regions located solely in the frontal, temporal and occipital parts of the brain.

Algorithms		$\mu_{\text{performance}}$	$\sigma_{\text{performance}}$
Logistic Regression (L1)	**hyper**	**0.670**	**(0.053**
	hypo	0.466	0.051
K-Nearest Neighbors	hyper	0.615	0.045
	hypo	0.618	0.030
Decision Tree	hyper	0.600	0.072
	hypo	0.478	0.062
Ridge	hyper	0.646	0.050
	hypo	0.509	0.043
SVM	hyper	0.657	0.043
	hypo	0.583	0.041
Gaussian Naive Bayes	hyper	0.623	0.049
	hypo	0.596	0.035

Table 1. Classification results obtained with NBS-SNI ($d = 1$) with the closeness centrality as the node property, with parameters $p_{\text{node}} = 0.00001$ and $t_{\text{edge}} = 2$. The average number of functional edges extracted by the method across folds are $k_{\text{hyper}} = 188 \pm 20$ and $k_{\text{hypo}} = 121 \pm 19$.

A

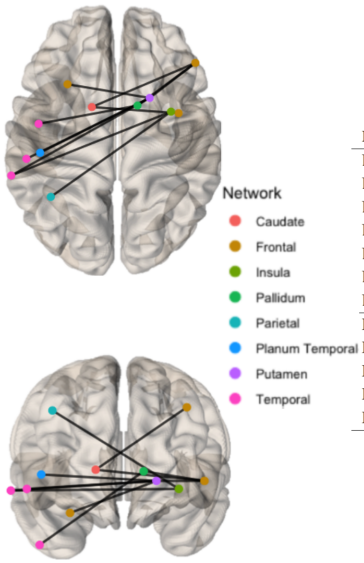

B

Node	Region	Hemisphere	Degree
Left Frontal Orbital Cortex	Frontal	L	1.0
Left Planum Temporale	Planum Temporale	L	1.0
Left Middle Temporal Gyrus post. div.	Temporal	L	2.0
Left Middle Temporal Gyrus post. div.	Temporal	L	1.0
Left Inferior Temporal Gyrus ant. div.	Temporal	L	1.0
Left Angular Gyrus	Parietal	L	1.0
Left Caudate	Caudate	L	2.0
Right Precentral Gyrus	Frontal	R	1.0
Right Inferior Frontal Gyrus pars triangularis	Frontal	R	3.0
Right Insular Cortex	Insula	R	2.0
Right Pallidum	Pallidum	R	2.0
Right Putamen	Putamen	R	5.0

Figure 7. (A) Top and front views of the hypoconnected component extracted with the method NBS-SNI using the closeness centrality as the nodal property investigated and the Logistic regression algorithm to perform predictions. 23 edges which had a final prediction weight of 1 after scaling (0.673 before scaling) were retained. Within these 23 edges, the connected component of 11 edges shown was identified. (B) Nodal degree of the nodes present in the hypoconnected component on the left.

Algorithms		$\mu_{\text{performance}}$	$\sigma_{\text{performance}}$
Logistic Regression (L1)	hyper	0.564	0.038
	hypo	0.598	0.047
K-Nearest Neighbors	hyper	0.619	0.041
	hypo	0.668	0.036
Decision Tree	hyper	0.496	0.071
	hypo	0.448	0.067
Ridge	hyper	0.534	0.049
	hypo	**0.734**	**0.039**
SVM	hyper	0.605	0.034
	hypo	0.682	0.042
Gaussian Naive Bayes	hyper	0.588	0.041
	hypo	0.646	0.038

Table 2. Classification results obtained with NBS-SNI ($d = 1$) with current flow closeness centrality as the node property, with parameters $p_{\text{node}} = 0.000025$ and $t_{\text{edge}} = 2$. The average number of functional edges extracted by the method across folds are $k_{\text{hyper}} = 298 \pm 32$ and $k_{\text{hypo}} = 227 \pm 26$.

A

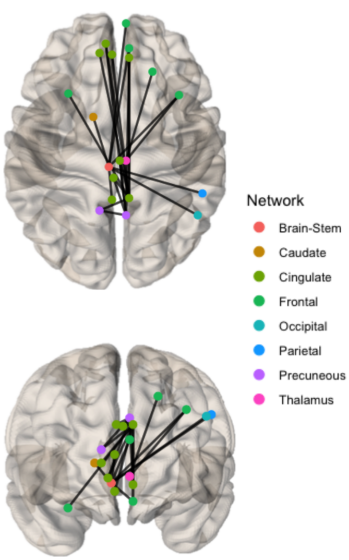

B

Node	Region	Hemisphere	Degree
Brain-Stem	Brain-Stem	-	7
Left Frontal Orbital Cortex	Frontal	L	1
Left Cingulate Gyrus anterior division	Cingulate	L	1
Left Paracingulate Gyrus	Cingulate	L	2
Left Cingulate Gyrus posterior division	Cingulate	L	2
Left Paracingulate Gyrus	Cingulate	L	1
Left Cingulate Gyrus posterior division	Cingulate	L	1
Left Caudate	Caudate	L	1
Left Precuneous Cortex	Precuneous	L	2
Right Middle Frontal Gyrus	Frontal	R	2
Right Superior Frontal Gyrus	Frontal	R	1
Right Frontal Medial Cortex	Frontal	R	2
Right Frontal Pole	Frontal	R	1
Right Thalamus	Thalamus	R	2
Right Cingulate Gyrus posterior division	Cingulate	R	9
Right Paracingulate Gyrus	Cingulate	R	2
Right Cingulate Gyrus posterior division	Cingulate	R	2
Right Supramarginal Gyrus posterior division	Parietal	R	1
Right Lateral Occipital Cortex superior division	Occipital	R	1
Right Precuneous Cortex	Precuneous	R	5

Figure 8. (A) Using the current flow closeness centrality, the hypoconnected subnetwork was extracted with the method NBS-SNI and the Ridge classifier algorithm. 43 edges which had a final prediction weight ≥ 0.99 after scaling were retained. Within these 43 edges, the connected component of 23 edges shown (top and front views) was found. (B) Nodal degree of the nodes present in the hypoconnected subnetwork on the left.

Algorithms		$\mu_{\text{performance}}$	$\sigma_{\text{performance}}$
Logistic Regression (L1)	hyper	0.545	0.058
	hypo	0.565	0.0451
K-Nearest Neighbors	hyper	0.592	058
	hypo	0.623	0.051
Decision Tree	**hyper**	**0.704**	**0.063**
	hypo	0.617	0.08
Ridge	hyper	0.629	0.036
	hypo	0.501	0.07
SVM	hyper	0.604	0.044
	hypo	0.599	0.053
Gaussian Naive Bayes	hyper	0.603	0.040
	hypo	0.603	0.050

Table 3. Classification results obtained with NBS-SNI ($d = 1$) with local information dimension (LID) as the node property, with parameters $p_{\text{node}} = 0.005$ and $t_{\text{edge}} = 2.15$. The average number of functional edges extracted by the method across folds are $k_{\text{hyper}} = 124 \pm 18$ and $k_{\text{hypo}} = 98 \pm 30$.

A

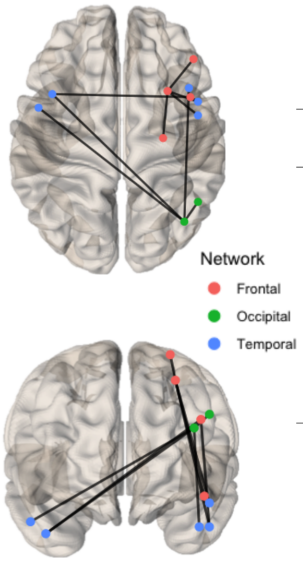

B

Node	Region	Hemisphere	Degree
Left Middle Temporal Gyrus ant. div.	Temporal	L	1.0
Left Temporal Pole	Temporal	L	2.0
Right Precentral Gyrus	Frontal	R	1.0
Right Precentral Gyrus	Frontal	R	2.0
Right Middle Frontal Gyrus	Frontal	R	4.0
Right Frontal Pole	Frontal	R	1.0
Right Temporal Pole	Temporal	R	2.0
Right Superior Temporal Gyrus ant. div.	Temporal	R	1.0
Right Temporal Pole	Temporal	R	1.0
Right Lateral Occipital Cortex sup. div.	Occipital	R	4.0
Right Lateral Occipital Cortex sup. div.	Occipital	R	1.0

Figure 9. (A) Using the local information dimension (LID) the hyperconnected subnetwork was extracted with the method NBS-SNI and the Decision tree classifier algorithm. 17 edges which had a final prediction weight ≥ 0.99 after scaling were retained. Within these 17 edges, the connected component of 10 edges was identified. (B) Nodal degree in the hyperconnected subnetwork depicted on the left. Note that due to the large number of nodes present in the component, either only one node per region, or nodes with a degree greater than one are included in this table.

Algorithms		$\mu_{\text{performance}}$	$\sigma_{\text{performance}}$
Logistic Regression (L1)	hyper	0.461	0.033
	hypo	0.570	0.026
K-Nearest Neighbors	hyper	0.606	0.039
	hypo	0.630	0.031
Decision Tree	hyper	0.547	0.063
	hypo	0.510	0.059
Ridge	hyper	0.554	0.052
	hypo	0.562	0.044
SVM	hyper	0.598	0.033
	hypo	0.615	0.031
Gaussian Naive Bayes	hyper	0.604	0.042
	hypo	**0.639**	**0.026**

Table 4. Classification results obtained with the standard NBS with parameter $t_{\text{edge}} = 2.5$. The average number of functional edges extracted by the method across folds are $k_{\text{hyper}} = 347 \pm 37$ and $k_{\text{hypo}} = 319 \pm 33$.

Comparison of predictions performances with NBS

Finally, the standard NBS was also employed to perform predictions. A range of parameter thresholds t_{edge} was tried, with $t_{\text{edge}} = 2.5$ being the one that yielded the best prediction performance. The classification results are presented in table 4. The best prediction performance was yielded by the Gaussian Naive Bayes algorithm $\mu_{\text{performance}} = 0.639 \pm 0.026$ with the hypoconnected subnetwork, containing on average $k_{\text{hypo}} = 319 \pm 33$ edges.

5 CONCLUSION

In this paper, a method called NBS-SNI was introduced, which is an extension to the Network-based statistic (NBS; Zalesky et al. 2010). By being supplemented with the structural network representation, NBS-SNI can be used to identify abnormal functional connections and perform classification in case-control studies. More precisely, the framework that we presented sets to find the most important brain regions according to a certain node property of interest (for e.g., centrality measures), and probes for abnormal connectivity within or surrounding these thought-to-be important actors in the communication pathways of the brain. NBS-SNI is most well suited for cases when the contrast-to-noise ratio is relatively small in the contrast of interest. Furthermore, these connections forming the contrast should interconnect nodes that have some property which makes them stand out compared to other nodes; in that regime NBS-SNI is expected to offer a greater statistical resolution power than NBS by providing a tighter control of the family-wise error rate.

Using synthetic data, ROC curves were presented to show the regimes for which NBS-SNI is expected to offer a gain in statistical resolution over NBS at identifying a contrast. NBS-SNI was also applied on a real case-control dataset of 29 individuals diagnosed with ASD and 19 healthy individuals, containing both the structural and functional network representation of each individual. Using both network representations with NBS-SNI, a classification performance of 73% was obtained using the current flow closeness centrality

of nodes, while the best performance obtained with NBS using only the functional representation was 64%.

We also want to emphasize the notion that NBS-SNI is a general framework, and its uses may not be limited to the ones presented in this paper. The choice of node properties to investigate is numerous. Using node properties such as centrality measures, as it was done in this paper, seems most appropriate for large scale neuroimaging data, since the volume of the parcellated brain regions does not vary much at this scale (Simpson et al., 2013), which is essential for the relevance of the subsequent statistical analysis undertaken with NBS-SNI, which relies on a close correspondence between nodes across individuals. Another avenue for the method could be to incorporate aggregated microscale information into this framework as the node properties. Interest and recent advances in multiscale brain imaging could provide researchers with a more comprehensive understanding of the structure-function relationships (Abdeladim et al., 2019; Desjardins et al., 2019; Schirner, McIntosh, Jirsa, Deco, & Ritter, 2018; Schulz et al., 2012). Indeed, such research endeavours should involve multiscale approaches, since the relationship between structure and function is believed to be heterogeneous across the brain, due to the different physiological and molecular micro-properties of its different constituents (Khambhati, Sizemore, Betzel, & Bassett, 2018; Lariviere et al., 2019; Murphy et al., 2016; Suárez et al., 2020; van den Heuvel & Yeo, 2017). Examples of microscale information that could be incorporated in a framework like NBS-SNI include gene expression, cytoarchitechture, neuron morphology, glial cells density/type, myelin content, etc. Animals such as rats and mice are well disposed to be subject to such multiscale neuroimaging studies (Desjardins et al., 2019; Schulz et al., 2012). These kinds of datasets will become more abundant in the coming years, and we believe NBS-SNI will be a useful tool to leverage them.

Besides, diagnosis of certain brain conditions such as the autism spectrum disorder (ASD) can be challenging for clinical doctors, but also for the patients and their relatives. For example, a survey from 2016 in the UK shows that parents wait an average of 3.5 years between the time they approach clinical doctors to when they receive a diagnostic of autism for their children (Crane, Chester, Goddard, Henry, & Hill, 2016). Further, there are criticisms regarding the different diagnostic criteria for the different subtypes of the condition within the wider definition of the autism spectrum disorder (Tidmarsh & Volkmar, 2003). This is likely due to the overlap between the different subtypes of ASD; some are not well delineated, perhaps owing to the lack of a systematic quantification of the symptoms, brain morphology and functional activity signatures implicated in the condition. We advance that network based approaches applied in neuroscience, such as the method proposed in this work are well positioned to address these issues, and could broaden the clinical doctors' assessments with quantitative features.

Finally, another promising avenue for patients affected by a neurodevelopmental disorder who are refractory to conventional pharmacological treatment (Lindenmayer, 2000; Siskind, McCartney, Goldschlager, & Kisely, n.d.) lies in alternative therapeutic approaches, such as transcranial magnetic stimulation (TMS) (Cash et al., 2021). This approach is becoming more precise in the targeting of the brain region(s) to stimulate. We posit that the identification of abnormal functional connections between influential actors in brain networks are promising candidates for customized targeted TMS treatments.

REFERENCES

Abdeladim, L., Matho, K. S., Clavreul, S., Mahou, P., Sintes, J.-M., Solinas, X., … others (2019). Multicolor multiscale brain imaging with chromatic multiphoton serial microscopy. *Nat. Commun.*, *10*, 1662. doi: 10.1038/s41467-019-09552-9

Akarca, D., Vértes, P. E., Bullmore, E. T., & Astle, D. E. (2021). A generative network model of neurodevelopmental diversity in structural brain organization. *Nat. Commun.*, *12*, 4216. doi: 10.1038/s41467-021-24430-z

Baum, G. L., Ciric, R., Roalf, D. R., Betzel, R. F., Moore, T. M., Shinohara, R. T., … Satterthwaite, T. D. (2017). Modular Segregation of Structural Brain Networks Supports the Development of Executive Function in Youth. *Curr. Biol.*, *27*, 1561-1572.e8. doi: 10.1016/j.cub.2017.04.051

Baum, G. L., Cui, Z., Roalf, D. R., Ciric, R., Betzel, R. F., Larsen, B., … Satterthwaite, T. D. (2020). Development of structure–function coupling in human brain networks during youth. *Proc. Natl. Acad. Sci. U.S.A.*, *117*, 771–778. doi: 10.1073/pnas.1912034117

Betzel, R. F., Avena-Koenigsberger, A., Goñi, J., He, Y., de Reus, M. A., Griffa, A., … Sporns, O. (2016). Generative models of the human connectome. *NeuroImage*, *124*, 1054-1064. doi: 10.1016/j.neuroimage.2015.09.041

Brandes, U., Borgatti, S. P., & Freeman, L. C. (2016). Maintaining the duality of closeness and betweenness centrality. *Soc. Networks*, *44*, 153–159. doi: 10.1016/j.socnet.2015.08.003

Cash, R. F. H., Weigand, A., Zalesky, A., Siddiqi, S. H., Downar, J., Fitzgerald, P. B., & Fox, M. D. (2021). Using Brain Imaging to Improve Spatial Targeting of Transcranial Magnetic Stimulation for Depression. *Biol. Psychiatry*, *90*, 689–700. doi: 10.1016/j.biopsych.2020.05.033

Cocchi, L., Harding, I. H., Lord, A., Pantelis, C., Yucel, M., & Zalesky, A. (2014). Disruption of structure–function coupling in the schizophrenia connectome. *NeuroImage Clin*, *4*, 779–787. doi: 10.1016/j.nicl.2014.05.004

Crane, L., Chester, J. W., Goddard, L., Henry, L. A., & Hill, E. (2016). Experiences of autism diagnosis: A survey of over 1000 parents in the United Kingdom. *Autism*, *20*, 153–162. doi: 10.1177/1362361315573636

Desjardins, M., Kılıç, K., Thunemann, M., Mateo, C., Holland, D., Ferri, C. G. L., … Devor, A. (2019). Awake Mouse Imaging: From Two-Photon Microscopy to Blood Oxygen Level–Dependent Functional Magnetic Resonance Imaging. *Biol. Psychiatry Cogn. Neurosci. Neuroimaging*, *4*, 533–542. doi: 10.1016/j.bpsc.2018.12.002

Honey, C. J., Thivierge, J.-P., & Sporns, O. (2010). Can structure predict function in the human brain? *NeuroImage*, *52*, 766–776. doi: 10.1016/j.neuroimage.2010.01.071

Khambhati, A. N., Sizemore, A. E., Betzel, R. F., & Bassett, D. S. (2018). Modeling and interpreting mesoscale network dynamics. *NeuroImage*, *180*, 337-349. doi: 10.1016/j.neuroimage.2017.06.029

Lariviere, S., Vos de Wael, R., Paquola, C., Hong, S.-J., Mišić, B., Bernasconi, N., … Bernhardt, B. C. (2019). Microstructure-informed connectomics: enriching large-scale descriptions of healthy and diseased brains. *Brain Connect.*, *9*. doi: 10.1089/brain.2018.0587

Lindenmayer, J.-P. (2000). Treatment refractory schizophrenia. *Psychiatric Quarterly*, *71*(4), 373–384. doi: https://doi.org/10.1023/A:1004640408501

Murphy, A. C., Gu, S., Khambhati, A. N., Wymbs, N. F., Grafton, S. T., Satterthwaite, T. D., & Bassett, D. S. (2016). Explicitly linking regional activation and function connectivity: Community structure of weighted networks with continuous annotation. *arXiv*, 1611.07962. doi: 10.48550/arXiv.1611.07962

Newman, M. E. J. (2018). *Networks*. Oxford University Press.

Park, H.-J., & Friston, K. (2013). Structural and Functional Brain Networks: From Connections to Cognition. *Science*, *342*, 1238411. doi: 10.1126/science.1238411

Pedregosa, F., Varoquaux, G., Gramfort, A., Michel, V., Thirion, B., Grisel, O., … Duchesnay, É. (2011). Scikit-learn: Machine Learning in Python. *J. Mach. Learn. Res.*, *12*, 2825–2830.

Pessoa, L. (2014). Understanding brain networks and brain organization. *Phys. Life Rev.*, *11*, 400–435. doi: 10.1016/j.plrev.2014.03.005

Power, J. D., Cohen, A. L., Nelson, S. M., Wig, G. S., Barnes, K. A., Church, J. A., … Petersen, S. E. (2011). Functional network organization of the human brain. *Neuron*, *72*, 665–78. doi: 10.1016/j.neuron.2011.09.006

Rudie, J. D., Brown, J. A., Beck-Pancer, D., Hernandez, L. M., Dennis, E. L., Thompson, P. M., … Dapretto, M. (2013). Altered functional and structural brain network organization in autism. *NeuroImage Clin*, *2*, 79–94. doi: 10.1016/j.nicl.2012.11.006

Schirner, M., McIntosh, A. R., Jirsa, V., Deco, G., & Ritter, P. (2018). Inferring multi-scale neural mechanisms with brain network modelling. *eLife*, *7*, e28927. doi: 10.7554/eLife.28927

Schulz, K., Sydekum, E., Krueppel, R., Engelbrecht, C. J., Schlegel, F., Schröter, A., … Helmchen, F. (2012). Simultaneous BOLD fMRI and fiber-optic calcium recording in rat neocortex. *Nat. Methods*, *9*, 597–602. doi: 10.1038/nmeth.2013

Serin, E., Zalesky, A., Matory, A., Walter, H., & Kruschwitz, J. D. (2021). NBS-Predict: A prediction-based extension of the network-based statistic. *NeuroImage*, *244*, 118625. doi: 10.1016/j.neuroimage.2021.118625

Silva, F. N., & da F. Costa, L. (2013). Local Dimension of Complex Networks. *arXiv*, 1209.2476. doi: 10.48550/arXiv.1209.2476

Simpson, S., Lyday, R., Hayasaka, S., Marsh, A., & Laurienti, P. (2013). A permutation testing framework to compare groups of brain networks. *Front. Comput. Neurosci.*, *7*, 171. doi: 10.3389/fncom.2013.00171

Siskind, D., McCartney, L., Goldschlager, R., & Kisely, S. (n.d.). *British Journal of Psychiatry*, 385–392. doi: 10.1192/bjp.bp.115.177261

Sporns, O., & Kötter, R. (2004). Motifs in Brain Networks. *PLOS Biol.*, *2*, e369. doi: 10.1371/journal.pbio.0020369

Stephenson, K., & Zelen, M. (1989). Rethinking centrality: Methods and examples. *Soc. Networks*, *11*, 1–37. doi: 10.1016/0378-8733(89)90016-6

Suárez, L. E., Markello, R. D., Betzel, R. F., & Misic, B. (2020). Linking Structure and Function in Macroscale Brain Networks. *Trends Cogn. Sci.*, *24*, 302–315. doi: 10.1016/j.tics.2020.01.008

Tidmarsh, L., & Volkmar, F. R. (2003). Diagnosis and Epidemiology of Autism Spectrum Disorders. *Can. J. Psychiatry*, *48*, 517–525. doi: 10.1177/070674370304800803

van den Heuvel, M. P., & Yeo, B. T. (2017). A spotlight on bridging microscale and macroscale human brain architecture. *Neuron*, *93*, 1248-1251. doi: 10.1016/j.neuron.2017.02.048

Wen, T., & Deng, Y. (2020). Identification of influencers in complex networks by local information dimensionality. *Inf. Sci.*, *512*, 549–562. doi: 10.1016/j.ins.2019.10.003

Witvliet, D., Mulcahy, B., Mitchell, J. K., Meirovitch, Y., Berger, D. R., Wu, Y., … Zhen, M. (2021). Connectomes across development reveal principles of brain maturation. *Nature*, *596*, 257–261. doi: 10.1038/s41586-021-03778-8

Zalesky, A., Fornito, A., & Bullmore, E. T. (2010). Network-based statistic: Identifying differences in brain networks. *NeuroImage*, *53*, 1197–1207. doi: 10.1016/j.neuroimage.2010.06.041